Hindawi Publishing Corporation
Advances in Mathematical Physics
Volume 2015, Article ID 657620, 9 pages
http://dx.doi.org/10.1155/2015/657620

Research Article

Anisotropic Characteristics of Turbulence Dissipation in Swirling Flow: A Direct Numerical Simulation Study

Xingtuan Yang,[1] Nan Gui,[1,2] Gongnan Xie,[3] Jie Yan,[4] Jiyuan Tu,[1,5] and Shengyao Jiang[1]

[1] *Institute of Nuclear and New Energy Technology and Key Laboratory of Advanced Reactor Engineering and Safety, Ministry of Education, Beijing 100084, China*
[2] *College of Mechanical and Transportation Engineering, China University of Petroleum, Beijing 102249, China*
[3] *School of Mechanical Engineering, Northwestern Polytechnical University, Xi'an 710072, China*
[4] *China Academy of Space Technology, Beijing 100094, China*
[5] *School of Aerospace, Mechanical & Manufacturing Engineering, RMIT University, Melbourne, VIC 3083, Australia*

Correspondence should be addressed to Shengyao Jiang; shengyaojiang@sina.com

Received 7 August 2014; Revised 13 December 2014; Accepted 15 December 2014

Academic Editor: Alina Adriana Minea

This study investigates the anisotropic characteristics of turbulent energy dissipation rate in a rotating jet flow via direct numerical simulation. The turbulent energy dissipation tensor, including its eigenvalues in the swirling flows with different rotating velocities, is analyzed to investigate the anisotropic characteristics of turbulence and dissipation. In addition, the probability density function of the eigenvalues of turbulence dissipation tensor is presented. The isotropic subrange of PDF always exists in swirling flows relevant to small-scale vortex structure. Thus, with remarkable large-scale vortex breakdown, the isotropic subrange of PDF is reduced in strongly swirling flows, and anisotropic energy dissipation is proven to exist in the core region of the vortex breakdown. More specifically, strong anisotropic turbulence dissipation occurs concentratively in the vortex breakdown region, whereas nearly isotropic turbulence dissipation occurs dispersively in the peripheral region of the strong swirling flows.

1. Introduction

Vortex breakdown is an intriguing and important phenomenon that occurs in a variety of natural and technological swirling flows, for example, swirling combustor, cyclone, bathtub vortex, hurricanes and tornadoes, and spiral galaxies. In general, the appearance of swirl is caused by the impartment of rotating motion upon the jet which makes the flow more complicated and has been widely studied in the literature [1–10]. The scope of this study does not include summarizing existing vast literature of swirling flow investigation; thus, only a few investigations on this topic were covered.

For example, Chen and Sun [1] addressed the nonlinear 3D instability of a specific type of viscous swirling flow, the Ossen vortex, by using direct numerical simulation at Re = 5000. They considered the global optimal perturbation as the initial perturbation and characterized different flow regimes in axisymmetric cases. Wang and Chen [2] studied vortex breakdown by solving 3D unsteady Navier-Stokes equations for swirling pipe flows, including the flow structures in the bubble domain and the tails behind the breakdown vortex. Moreover, Shtern et al. [4] studied symmetry breaking in a meridional steady motion of viscous incompressible fluids using the laminar axisymmetric "vortex dynamo." They demonstrated the feasibility of a supercritical pitchfork bifurcation from an initially nonswirling flow to a steady swirling regime, as Re exceeds a critical value. In addition, with regard to model study, di Pierro and Abid [5] investigated modeled inviscid swirling flows, addressing the weak variation of axial and azimuthal velocities. They checked the asymptotic results using numerically computed growth rates of linearized Euler equations for a family of variable-density Batchelor-like vortices as base flows and so forth.

Turbulent flows are well known to have scientific and practical importance. However, the full spectrums of the length and time scales of turbulent flows are impossible to

solve via computer simulation. Thus, some types of modeling for Reynolds stresses are needed to simulate high Reynolds turbulence. For example, the turbulent kinetic energy and dissipation are involved in the standard form of the two-equation Reynolds stress turbulence model based on the Boussinesq-type approximation [11]:

$$\tau_{ij} = -\frac{2}{3}K\delta_{ij} + \nu_T\left(\frac{\partial U_i}{\partial x_j} + \frac{\partial U_j}{\partial x_i}\right), \quad (1)$$

where K is the turbulent kinetic energy, U_i is the time-averaged velocity, and ν_T is the isotropic turbulent viscosity. However, this turbulence model is fairly ineffective in simulating anisotropic turbulence due to the theoretical deficiency for anisotropic nature of turbulent motions, although it is widely applied in engineering. Thus, numerous studies have been carried out to further understand the physical aspects of anisotropic turbulent flows and vortex dynamics [12–14].

In conclusion, swirling flow is present in anisotropic turbulent flows and is a striking and intriguing case of the generation and breakdown of strong vortices. However, the characteristics of the anisotropic nature of turbulent motion and energy dissipation are not clear, especially in strong swirling turbulent jet flows. Thus, the present study carried out a numerical study on the characteristics of energy dissipation tensor in a rotating jet flow. Three swirling numbers are used, corresponding to weak, intermediate, and strong swirling levels. The relations of the components of energy dissipation corresponding to normal and shearing turbulent fluctuations are explored, including their probability density function. The specific locations in the swirling flows, corresponding to the regions of extremely anisotropic and nearly isotropic turbulent dissipation, are also presented. The locations indicate the correlation of anisotropic turbulence dissipation to the large-scale structure of vortex breakdown and the correlation of isotropic turbulence dissipation to small-scale vortices.

2. Numerical Description

2.1. Governing Equations. For incompressible Newtonian fluids, the governing equations can be expressed in dimensionless form as follows:

$$\nabla \cdot \mathbf{u} = 0 \quad (2)$$

$$\partial_t \mathbf{u} + \mathbf{u} \cdot \nabla \mathbf{u} = -\nabla p + \frac{1}{\mathrm{Re}}\Delta \mathbf{u}, \quad (3)$$

where $\mathbf{u}$ and p are the velocity and pressure, respectively. $\mathrm{Re} = U_0 \cdot d/\nu$ is the Reynolds number, in which U_0 is the inflow velocity, d is the jet diameter at the inlet, and ν is the kinematic viscosity.

Equations (2) and (3) deal with a three-dimensional time-dependent flow problem without body force. To solve them, the finite difference method is applied, where the convection term is discretized by upwind compact schemes [15], and the space derivatives and pressure-gradient terms are discretized by fourth-order compact difference schemes [16], respectively. The third-order explicit schemes are used to deal with the boundary points and to maintain the global fourth-order spatial accuracy. The time stepping process is integrated by using the fourth-order Runge-Kutta schemes [17]. The pressure-Poisson equation is solved to obtain pressure via the fourth-order finite difference method [18]. The validation of the codes has been done in a recently published work on swirling flows [19].

Table 1: Typical real values of variables used in the numerical simulation.

Scales of the flow domain (mm)	$20 * 10 * 10$
Scale of jet diameter d (mm)	1.0
Grids number $N_x * N_y * N_z$	$512 * 256 * 256$
Scale of resolution Δ (μm)	39
Mean inlet axial velocity U_0 (m/s)	71.71
Fluid density (kg/m^3)	1.29
Fluid viscosity (Pa·s)	$1.85 * 10^{-5}$
Inflow momentum thickness λ (/d)	1/20
Reynolds number Re	5000
Swirl number S	Case 1: 0.28; Case 2: 0.45; Case 3: 0.59;
Time step Δt	0.001
Number of simulation step N_s	20000

2.2. Boundary Conditions. As shown in Figure 1(a), the flow configuration contains a rectangular flow domain of $20d \times 10d \times 10d$, where d is the diameter of the jet inlet and the jets are injected from the inlet with a mean velocity U_0. The entire flow domain is discretized by $512 \times 256 \times 256$ Cartesian mesh grids, and the mesh scale is not larger than $\Delta x = 15.625\,\mu$m. The Kolmogorov length scale is estimated in the same order of the finest mesh scale, namely, $\eta \sim O(\Delta x)$ [19, 20]. According to the suggestion by Moin and Mahesh [21], the mesh scale in the same order of the Kolmogorov scale is fine enough to capture the smallest scale of turbulence. Thus, the grid testing procedure is omitted here. The time step is $\Delta t = 0.001$, and 20000 time steps are simulated for each case. The nonreflecting boundary condition is utilized for the outlet condition [22], and the sidewalls are set as nonslipping wall boundaries.

For axial inflow velocity, a hyperbolic tangent profile is used within the range of $|r - r^c| < d/2$:

$$u_x\left(r - r^c\right) = \frac{1}{2}\left[1 + \tanh\left(\frac{0.5 - \left|r - r^c\right|}{2\lambda}\right)\right], \quad (4)$$

where r^c is the center position of the jet. The reference system is centered at the inlet with $r^c = 0$. λ is the inflow momentum thickness (Table 1) and the ratio of the jet width to the inflow momentum thickness is $d/\lambda = 20$. For azimuthal inflow velocity, a polynomial expression is used; that is,

$$u_\theta = a_0 + a_1 r + a_2 r^2 + a_3 r^3 + a_4 r^4 + a_5 r^5, \quad (5)$$

where the coefficients a_i are listed in Table 2. The combined profiles of axial and azimuthal velocities are shown in

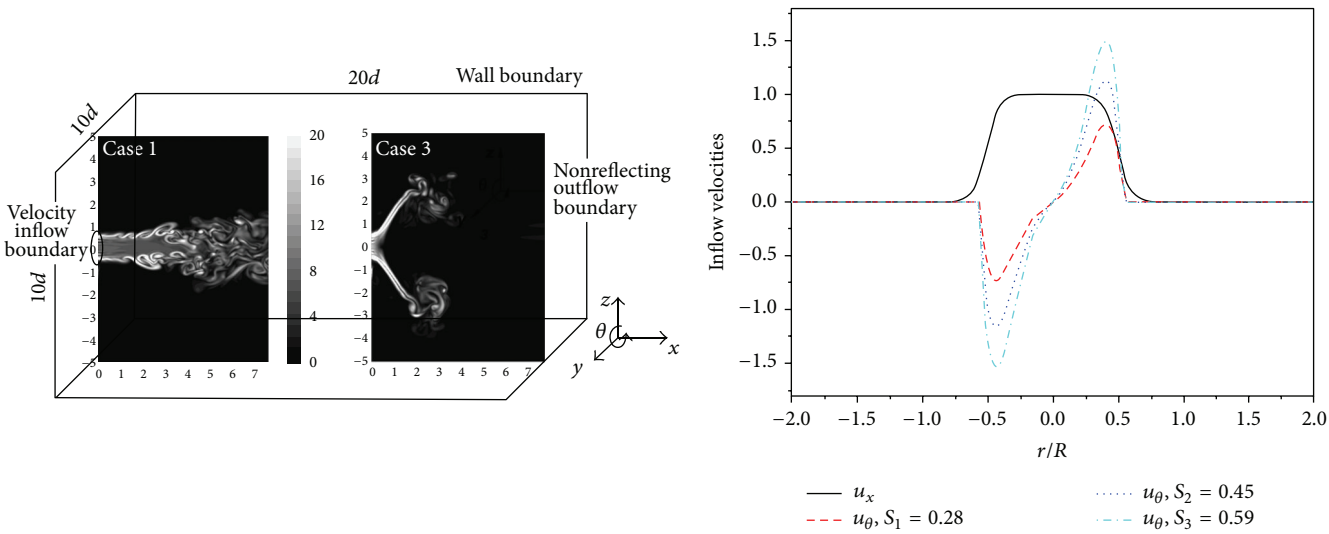

(a) (b)

Figure 1: Sketch of simulation setup: typical vortex streets (a) and inflow velocity profiles (b).

Table 2: Coefficients of the expressions for inflow velocity u_θ.

S_M	a_0	a_1	a_2	a_3	a_4	a_5
0.28	0	0.72	0.24	16.72	−1.40	−62.38
0.45	0	1.14	0.38	26.56	−2.22	−99.07
0.59	0	1.20	0.50	34.92	−2.92	−130.26

Figure 1(b). In addition, no initial turbulence is introduced to show the intrinsic full evolution of coherent vortex structures and interactions.

In addition, swirl number S is defined as the ratio of the axial flux of angular momentum to the axial momentum; that is,

$$S = \frac{2\int_0^{d/2} 2\pi r^2 u_x u_\theta dr}{d\int_0^{d/2} 2\pi r u_x^2 dr}. \tag{6}$$

Based on (4) and (5), three swirl numbers are used (Table 2). From the engineering viewpoint, $S = 0.28$ is considered as low swirl jets, whereas $S > 0.59$ is considered as strong swirling flows and $S = 0.45$ is intermediate.

2.3. Reynolds Stress Transport Equation. The Reynolds-averaged Navier-Stokes equation [23] is usually used to solve the turbulent flows in industrial scales:

$$\frac{\partial\langle u_i\rangle}{\partial x_i} = 0,$$

$$\frac{\partial\langle u_i\rangle}{\partial t} + \langle u_j\rangle\frac{\partial\langle u_i\rangle}{\partial x_j} = -\frac{\partial\langle p\rangle}{\partial x_i} + \frac{1}{\mathrm{Re}}\frac{\partial^2\langle u_i\rangle}{\partial x_j\partial x_j} - \frac{\partial\langle u_i' u_j'\rangle}{\partial x_j}, \tag{7}$$

where $\langle\cdot\rangle$ is the time-averaged operator. $\langle u_i' u_j'\rangle$ is the Reynolds stress tensor, which can be solved through the Reynolds stress transport equation and is given by

$$\begin{aligned}
&\frac{\partial\langle u_i' u_j'\rangle}{\partial t} + \langle u_k\rangle\frac{\partial\langle u_i' u_j'\rangle}{\partial x_k} \\
&\quad = -\langle u_i' u_k'\rangle\frac{\partial\langle u_j'\rangle}{\partial x_k} - \langle u_j' u_k'\rangle\frac{\partial\langle u_i'\rangle}{\partial x_k} \\
&\qquad + \left\langle p'\left(\frac{\partial u_i'}{\partial x_j} + \frac{\partial u_j'}{\partial x_i}\right)\right\rangle \\
&\qquad - \frac{\partial}{\partial x_k}\left(\langle p' u_i'\rangle\delta_{jk} + \langle p' u_j'\rangle\delta_{ik} + \langle u_i' u_j' u_k'\rangle\right. \\
&\qquad\qquad \left. - \frac{1}{\mathrm{Re}}\frac{\partial\langle u_i' u_j'\rangle}{\partial x_k}\right) \\
&\qquad - 2\frac{1}{\mathrm{Re}}\left\langle\frac{\partial u_i'}{\partial x_k}\frac{\partial u_j'}{\partial x_k}\right\rangle,
\end{aligned} \tag{8}$$

where $E_{ij} = 2(1/\mathrm{Re})\langle(\partial u_i'/\partial x_k)(\partial u_j'/\partial x_k)\rangle$ is the turbulent energy dissipation tensor. The Reynolds stress tensor

$$\langle u_i' u_j'\rangle = \begin{pmatrix} \langle u_1' u_1'\rangle & \langle u_1' u_2'\rangle & \langle u_1' u_3'\rangle \\ \langle u_2' u_1'\rangle & \langle u_2' u_2'\rangle & \langle u_2' u_3'\rangle \\ \langle u_3' u_1'\rangle & \langle u_3' u_2'\rangle & \langle u_3' u_3'\rangle \end{pmatrix} \tag{9}$$

is relevant to the dissipation of turbulent kinetic energy and is a symmetric positive definite tensor. Thus, it corresponds

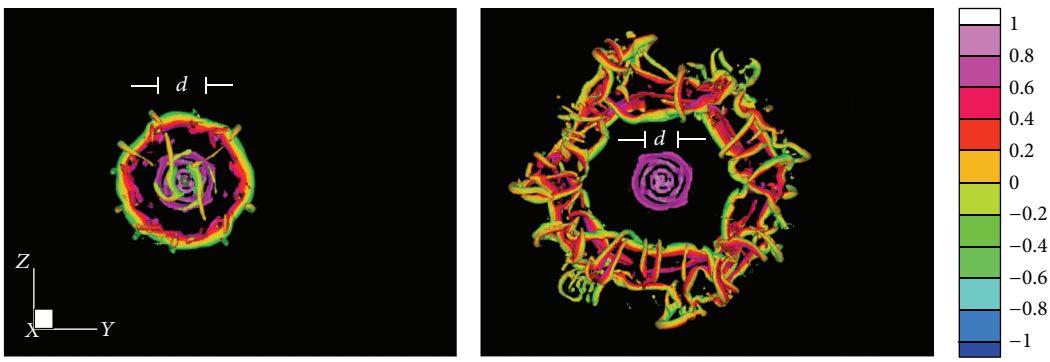

(a) (b)

Figure 2: Cross-sectional visualization of isovortex cores ($\lambda_2 = -50$, flood by axial velocity u_x) at $S_3 = 0.59$ at $t = 5$ (a) and $t = 15$ (b) in the central subregion.

to a diagonalizable matrix, and the anisotropic nature of the turbulent kinetic energy dissipation is indicated from the eigenvalues of the diagonalizable matrix. The anisotropic tensor has three unequal eigenvalues (i.e., at least two of them are unequal). Thus, the discrepancy between the eigenvalues, or equivalently, their relation and distribution, can indicate the anisotropic nature of turbulent kinetic energy dissipation in swirling flows.

3. Results and Discussions

3.1. Coherent Vortex Structures. The typical vortex structures are shown in Figure 1(a) when $S_1 = 0.28$ and $S_3 = 0.59$. For $S_1 = 0.28$, the Kelvin-Helmholtz instability dominates the vortex evolution due to the existence of a shear layer between the jets and ambient fluids. In contrast, the strong rotating effect dominates the evolution of the vortex structures for $S_3 = 0.59$. A cone-type vortex breakdown is established, and the K-H instability causes the breakdown of the "cone" feature from its terminal into the turbulent vortex streets.

Figure 2 shows that the typical cross-sectional visualizations of the vortex structures are visualized for $S_3 = 0.59$ (referring to the jet diameter d for the region width). The early evolution of the vortex for $t = 5$ (Figure 2(a)) has a full ring-type structure, with a positive stream-wise velocity ($u_x > 0$) in the inner side of the vortex ring (flood by red color in Figure 2(a) for $0.2 < u_x/U_0 < 0.8$) and a negative stream-wise velocity ($u_x < 0$) in the outer side of the ring (flood by blue color in Figure 2(a) for $-0.8 < u_x/U_0 < -0.2$). Central recirculation then occurs in the center of the jet, where the velocities are weakly negative. The ring structure of vortex for $t = 15$ (Figure 2(b)) evolves into more complicated structures. The diameter of the vortex ring tube becomes larger and starts to break down, and braid vortices are then formed. The complex vortex structures indicate the existence of turbulent vortex motions and dissipation of turbulent energy.

Based on the observations of Figure 2, the intrinsic characteristics of the vortex can be reflected by turbulent energy dissipations. However, these characteristics need to be explored to show the anisotropic/isotropic turbulent energy dissipation tensor and its correlation to vortex structures, among others.

3.2. Dissipation Tensor

3.2.1. Relation of Components of ε_{ij}. As previously mentioned, $E_{ij} = 2(1/\mathrm{Re})\langle \partial_k u_i' \, \partial_k u_j' \rangle$ dissipates turbulent kinetic energy $\langle u_i' \, u_j' \rangle$. E_{ij} is a symmetric positive definite tensor, which can be diagonalized. In general, three eigenvalues and three eigenvectors can be obtained in the diagonalization process. The eigenvectors are orthogonal and denote the three characteristic directions. The corresponding eigenvalues indicate the magnitudes of dissipation in each direction. Thus, an anisotropic tensor should have three (at least two) different eigenvalues, which correspond to different levels of dissipation in the three characteristic directions. In this way, the characteristics of anisotropic turbulent motion $\langle u_i' \, u_j' \rangle$ can be reflected by the characteristics of the eigenvalues and eigenvectors of dissipation tensor E_{ij}. $\varepsilon_{ij} = \langle \partial_k u_i' \, \partial_k u_j' \rangle$ was used because Re = 5000 is a constant.

First, Figure 3 illustrates the relation of the components of the tensor ε_{ij}. Each point in Figure 3 corresponds to the energy dissipation characteristics at each point location in the flow, with ε_{ii} part in the x-axis and $\varepsilon_{ij,i\neq j}$ part in the y-axis, because the dissipation tensor ε_{ij} has different values for different locations in the flow domain. The magnitude of $\varepsilon_{ij,i\neq j}$ fluctuation is almost the same as ε_{ii}, despite the swirling levels. Thus the energy dissipation of $\langle u_i' \, u_j' \rangle_{i\neq j}$ is almost the same as that of $\langle u_i' \, u_j' \rangle$. It is possibly caused by the transport of turbulent kinetic energy between $\langle u_i' \, u_j' \rangle_{i\neq j}$ and $\langle u_i' \, u_j' \rangle$, which results in dynamic balances of turbulent kinetic energy and dissipation between these types of turbulent fluctuation.

3.2.2. Distribution of the Eigenvalues. Second, tensor $\varepsilon_{ij} = \mathrm{diag}(\tilde{\varepsilon}_1, \tilde{\varepsilon}_2, \tilde{\varepsilon}_3)$ was diagonalized, where $\tilde{\varepsilon}_1$, $\tilde{\varepsilon}_2$, and $\tilde{\varepsilon}_3$ are the three eigenvalues of the tensor, which were sorted as $\tilde{\varepsilon}_1 \geq \tilde{\varepsilon}_2 \geq \tilde{\varepsilon}_3 \geq 0$ for simplicity. The distribution and relation of $\tilde{\varepsilon}_i$ are illustrated in Figure 4 using $S_1 = 0.28$ and $S_3 = 0.59$ for the case study. Figure 4(a) ($S_1 = 0.28$)

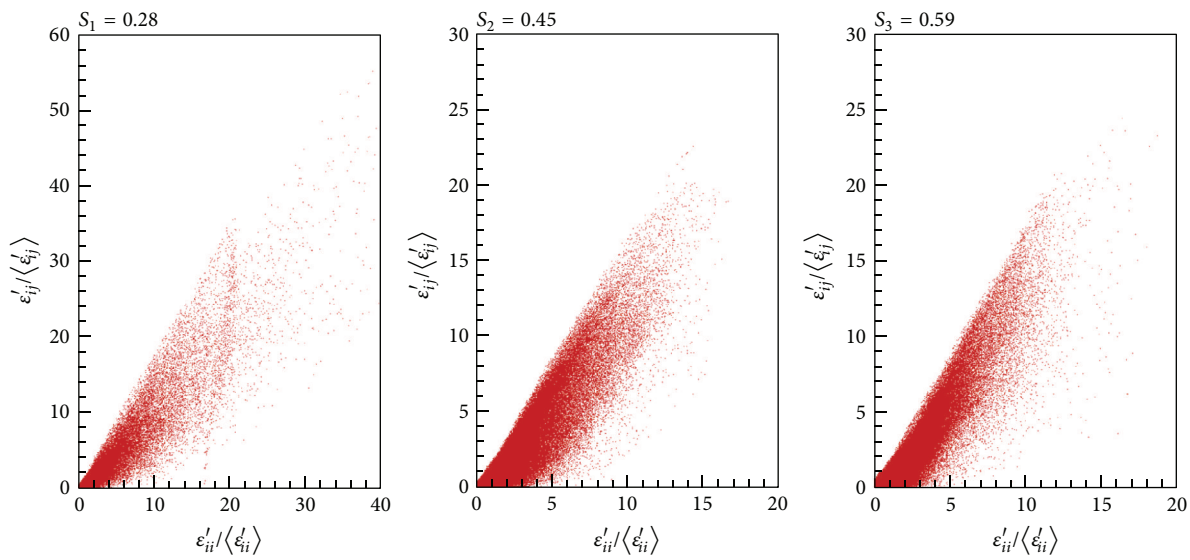

FIGURE 3: Relation of the components of the dissipation tensor ε_{ij} (ε_{ii} in the x-axis and $\varepsilon_{ij,i\neq j}$ in the y-axis, with $\varepsilon_{ii} = \varepsilon_{11} + \varepsilon_{22} + \varepsilon_{33}$ and $\varepsilon_{ij,i\neq j} = 2\{|\varepsilon_{12}| + |\varepsilon_{13}| + |\varepsilon_{23}|\}$, normalized by the root-mean-square values $\langle\varepsilon'_{ii}\rangle$ and $\langle\varepsilon'_{ij}\rangle$ of them, resp.).

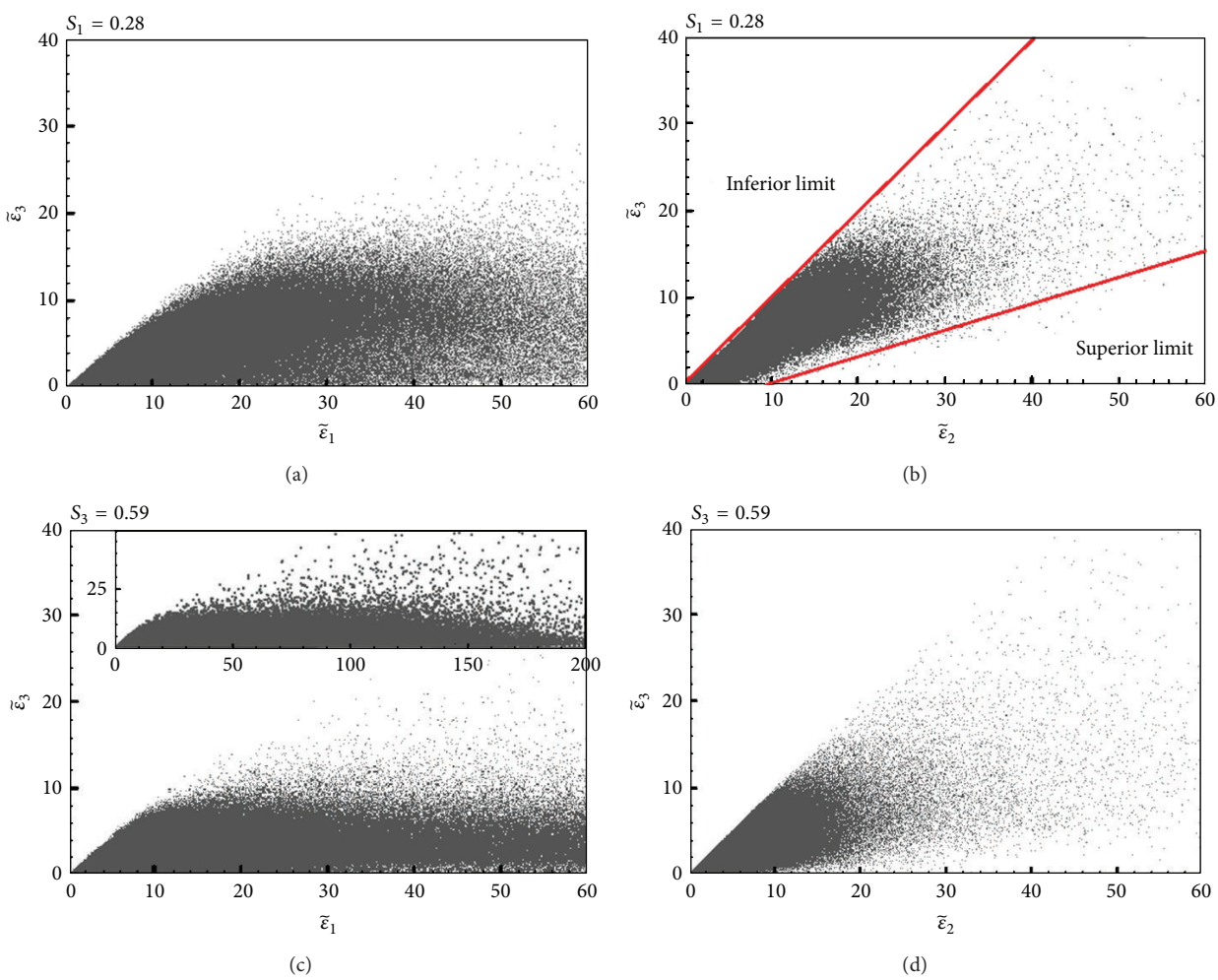

FIGURE 4: Relation of eigenvalues. (a) $S_1 = 0.28$, $\tilde{\varepsilon}_1 \sim \tilde{\varepsilon}_3$; (b) $S_1 = 0.28$, $\tilde{\varepsilon}_2 \sim \tilde{\varepsilon}_3$; (c) $S_3 = 0.59$, $\tilde{\varepsilon}_1 \sim \tilde{\varepsilon}_3$; (d) $S_3 = 0.59$, $\tilde{\varepsilon}_2 \sim \tilde{\varepsilon}_3$.

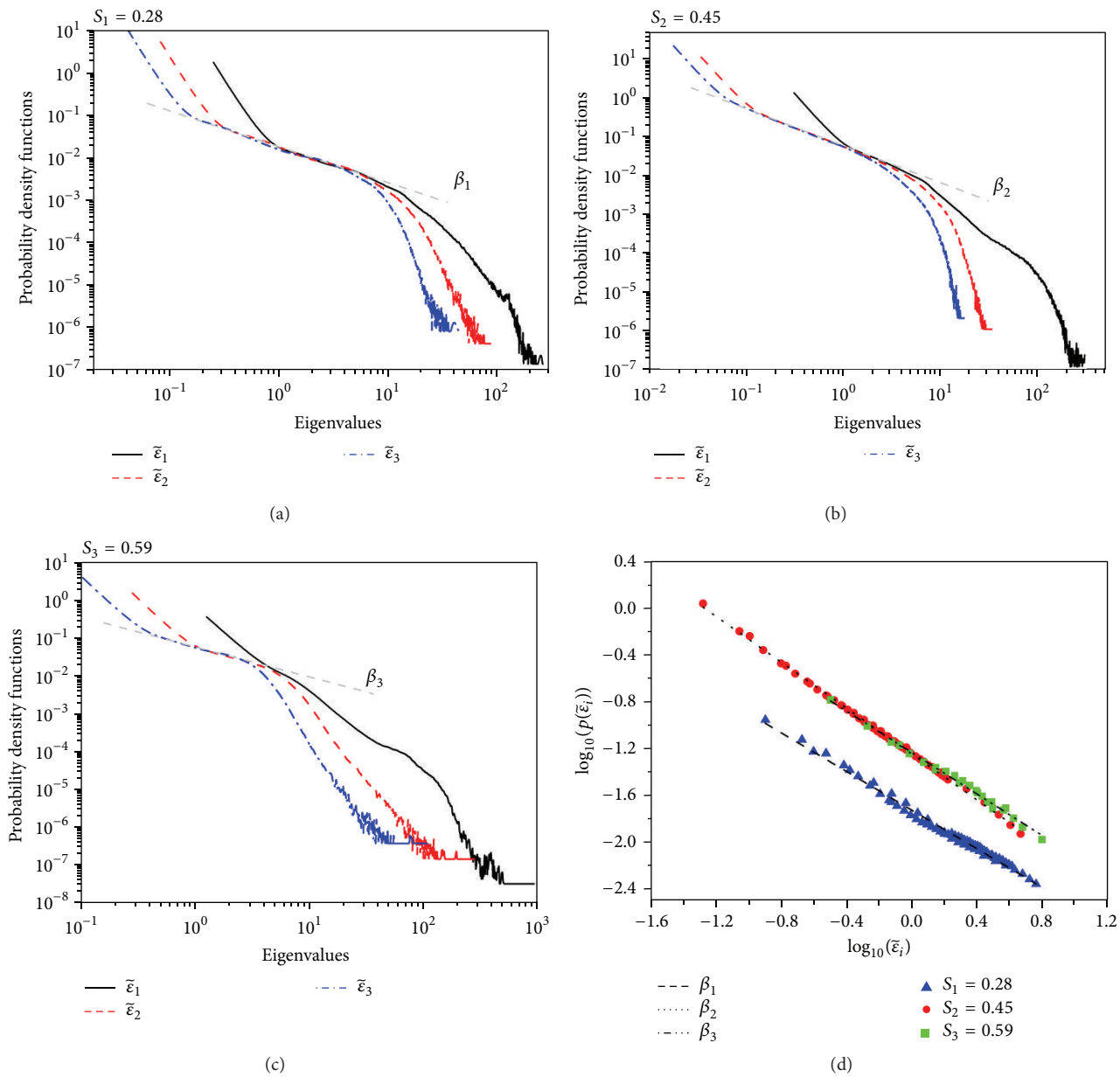

FIGURE 5: Probability density function $p(\varepsilon)$ for $S_1 = 0.28$ (a), $S_2 = 0.45$ (b), $S_3 = 0.59$ (c), and the linear subrange of them (d).

shows that the distribution of $(\tilde{\varepsilon}_1, \tilde{\varepsilon}_3)$ has a widespread area below the line of $\tilde{\varepsilon}_3 = \tilde{\varepsilon}_1$, indicating that it has $\tilde{\varepsilon}_1 > \tilde{\varepsilon}_3$ in most regions. Similar results were obtained in Figure 4(c) for $S_1 = 0.59$, and extreme discrepancies between $\tilde{\varepsilon}_3$ and $\tilde{\varepsilon}_1$ were observed, even as large as more than two or three orders. This observation indicates the extreme anisotropic characteristics of turbulent kinetic energy dissipation when the swirling level is sufficiently strong. Moreover, for $(\tilde{\varepsilon}_2, \tilde{\varepsilon}_3)$ (Figures 4(b) and 4(d)), although extreme events seem to be prohibited due to the possible existence of superior limit line, the distribution area is open and enlarged as $\tilde{\varepsilon}_2$ increases. In conclusion, Figure 4 shows the validation of the anisotropic characteristics of turbulent energy dissipation tensor, especially for strong swirling flows where extremely anisotropic events may occur.

3.2.3. Probability Density Functions $p(\tilde{\varepsilon}_i)$. Based on the combined distributions $(\tilde{\varepsilon}_i, \tilde{\varepsilon}_j)$ (e.g., $(\tilde{\varepsilon}_1, \tilde{\varepsilon}_3)$ and $(\tilde{\varepsilon}_2, \tilde{\varepsilon}_3)$), the probability density function $p(\tilde{\varepsilon}_i)$ (PDF) of one eigenvalue $\tilde{\varepsilon}_i$ can be obtained by integration of the other eigenvalue throughout the flow domain; that is, $p(\tilde{\varepsilon}_i) = \int p(\tilde{\varepsilon}_i, \tilde{\varepsilon}_j) d\tilde{\varepsilon}_j$. In general, PDF is defined as the concentration or density $\delta n(\tilde{\varepsilon}_i)$ of $\tilde{\varepsilon}_i$ located within the range of $(\tilde{\varepsilon}_i, \tilde{\varepsilon}_i + \delta\tilde{\varepsilon}_i)$; that is,

$$p(\tilde{\varepsilon}_i) = \frac{\delta n(\tilde{\varepsilon}_i)}{n \delta \tilde{\varepsilon}_i}, \tag{10}$$

where $n = \sum \delta n(\tilde{\varepsilon}_i)$ is the total number of points within the flow.

Figure 5 shows the PDFs for different swirling flows. For all the cases, that is, $S_1 = 0.28$ (Figure 5(a)), $S_2 = 0.45$ (Figure 5(b)), and $S_3 = 0.59$ (Figure 5(c)), the following

Table 3: Coefficients of the regression lines of β_1, β_2, and β_3.

	a	b	C
$S_1 = 0.28$	−0.823	−1.735	0.018
$S_2 = 0.45$	−0.976	−1.257	0.055
$S_3 = 0.59$	−0.883	−1.245	0.057

similar trends have been observed: (1) In most ranges, $p(\widetilde{\varepsilon}_1)|_{\widetilde{\varepsilon}_1=\widetilde{\varepsilon}_0} > p(\widetilde{\varepsilon}_2)|_{\widetilde{\varepsilon}_2=\widetilde{\varepsilon}_0} > p(\widetilde{\varepsilon}_3)|_{\widetilde{\varepsilon}_3=\widetilde{\varepsilon}_0}$ for the same eigenvalue of $\widetilde{\varepsilon}_0$ and $\widetilde{\varepsilon}_1|_{p_0} > \widetilde{\varepsilon}_2|_{p_0} > \widetilde{\varepsilon}_3|_{p_0}$ for the same value of PDF p_0, which means $\widetilde{\varepsilon}_1 > \widetilde{\varepsilon}_2 > \widetilde{\varepsilon}_3$ is true in most ranges; that is, the anisotropic turbulent dissipation occurs in most ranges. (2) A subrange of $\widetilde{\varepsilon}_i \in (e_l, e_h)$, which has $p(\widetilde{\varepsilon}_1) = p(\widetilde{\varepsilon}_2) = p(\widetilde{\varepsilon}_3)$, always exists, except that $p(\widetilde{\varepsilon}_1)$ for most strong swirling flows $S_3 = 0.59$. This phenomenon indicates the existence of subrange isotropic turbulent dissipation when the swirling level is not strong. On the other hand, turbulent energy dissipation in the major characteristic direction corresponding to the largest eigenvalues $\widetilde{\varepsilon}_1$ is always larger than the other characteristic directions for strong swirling flows ($S_3 \geq 0.59$), which indicates highly anisotropic turbulent energy dissipation characteristics in the main flow region.

Moreover, Figures 5(a) to 5(c) show that the isotropic subrange can be characterized by a regression line, designated as β_1, β_2, and β_3 for $S_1 = 0.28$, $S_2 = 0.45$, and $S_3 = 0.59$, respectively. The data in these subranges are illustrated in Figure 5(d) for clarity. Figure 5(d) shows a perfect linearity between $\log p(\widetilde{\varepsilon})$ and $\log(\widetilde{\varepsilon})$ for the isotropic subrange, which obtained the following equation using linear regression:

$$\log\left(p\left(\widetilde{\varepsilon}\right)\right) = a \cdot \log\left(\widetilde{\varepsilon}\right) + b, \quad \text{namely } p\left(\widetilde{\varepsilon}\right) = C \cdot \widetilde{\varepsilon}^{a}. \quad (11)$$

The regression coefficients are listed in Table 3, which shows that the power-law exits in the isotropic subrange of turbulent energy dissipation and that the power exponent is approximately −1 to −0.8. Moreover, the power-law occurs mainly for low turbulent energy dissipations, and the width of strong swirling flows is reduced. In other words, weak swirling flow has wider subranges of isotropic turbulent energy dissipation than the strong swirling flow and vice versa. This phenomenon indicates the significant role of swirling motion in augmenting the anisotropic characteristics of turbulence. To speak specifically, it is possible to assume that turbulent kinetic energy dissipation is more intensive and more nonlinear in strongly swirling flows than in weakly swirling flows. Therefore, the subranges of linear relations between probability distribution functions and eigenvalues of dissipation rates are reduced in strongly swirling flows compared to those in weakly swirling flows.

3.2.4. Correlation to Vortex Structures. Previously mentioned results are based on statistical analysis; thus visualizing the locations of extremely anisotropic and nearly isotropic turbulence dissipation should be helpful to further understand anisotropic turbulent swirling flows. For this reason, the data of $|\widetilde{\varepsilon}_1/\widetilde{\varepsilon}_3| > 100$ (see Figures 4(a) and 4(c)) and $-0.8 < \log\widetilde{\varepsilon}_1$, $\log\widetilde{\varepsilon}_2$, $\log\widetilde{\varepsilon}_3 < 0.4$ (see Figure 5(d) or equivalently $0.158 < \widetilde{\varepsilon}_1$, $\widetilde{\varepsilon}_2$, $\widetilde{\varepsilon}_3 < 2.5$) was extracted and the locations for these data in the background of vorticities of $S = 0.28$ and 0.59 were shown.

Figure 6 shows that the locations of extremely anisotropic turbulence dissipation (e.g., $|\widetilde{\varepsilon}_1/\widetilde{\varepsilon}_3| > 100$, designated by colored spheres) are concentrated in the central region of the jet (Figure 6(a)), corresponding to strong twisted vortices when the swirl level is low. On the other hand, the locations of nearly isotropic turbulence dissipation ($0.158 < \widetilde{\varepsilon}_1, \widetilde{\varepsilon}_2, \widetilde{\varepsilon}_3 < 2.5$) are dispersed in the peripheral region of the jet (Figure 6(b)), corresponding to the region with small-scale and weak turbulence. Moreover, the locations of extremely anisotropic turbulence dissipation are concentrated in the central region of vortex breakdown (Figure 6(c)), corresponding to strong swirling large-scale vortex structure when the swirl level is large. The locations of nearly isotropic turbulence dissipation are dispersed in the peripheral region of the vortex breakdown, such as strong small-scale vortices (Figure 6(d)).

Figure 6 conclusively shows that strong anisotropic turbulence dissipation occurs concentratively in the vortex breakdown region or is closely related to the large-scale vortex structure. On the other hand, nearly isotropic turbulence dissipation occurs dispersively in the peripheral region of the strong swirling flows, that is, closely related to small-scale vortices.

4. Conclusion

This work was carried out to investigate the physical aspects of anisotropic turbulent motions and dissipations in swirling flows. Based on the observation and analysis of the DNS results, the following results were found.

(1) Turbulent swirling jet flows have evident coherent structures relevant to the remarkable VB phenomenon and recirculation of the flows, which dominates anisotropic turbulent motions and dissipations.

(2) The evidently nonzero components of dissipation tensor relevant to $\langle u_i' \, u_j' \rangle_{i \neq j}$ validates the occurrence of anisotropic turbulent fluctuations and motions in swirling flows.

(3) With diagonalized dissipation tensor, the relation and distribution of the three eigenvalues show strong anisotropic characteristics of turbulent energy dissipation, especially in strong swirling flows.

(4) Based on the probability density functions, turbulent dissipation of swirling flows is anisotropic in most regions, but an isotropic subrange of turbulent dissipation still exists, especially for low swirling flows. On the contrary, the isotropic subrange of PDF is reduced for strong swirling flows. The power-law form of PDF for the isotropic subrange was obtained through linear regression.

(5) More importantly, strong anisotropic turbulence dissipation occurs concentratively in the vortex breakdown region or is closely related to the large-scale vortex structure, whereas the nearly isotropic turbulence dissipation occurs dispersively in the peripheral region of the strong swirling flows, that is, closely related to small-scale vortices.

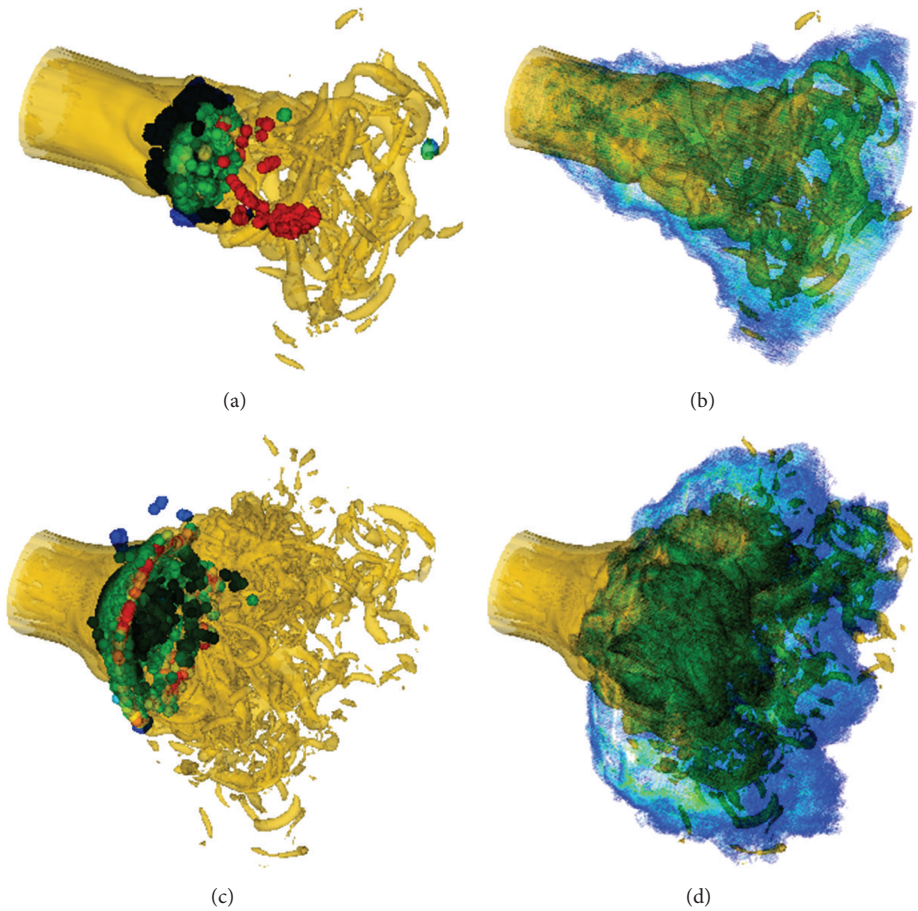

Figure 6: Locations of anisotropic turbulence dissipation ($|\tilde{\varepsilon}_1/\tilde{\varepsilon}_3| > 100$) for $S_1 = 0.28$ (a) and $S_3 = 0.59$ (c) and locations of nearly isotropic turbulence dissipation ($-0.8 < \log\tilde{\varepsilon}_1, \log\tilde{\varepsilon}_2, \log\tilde{\varepsilon}_3 < 0.4$ or $0.158 < \tilde{\varepsilon}_1, \tilde{\varepsilon}_2, \tilde{\varepsilon}_3 < 2.5$) for $S_1 = 0.28$ (b) and $S_3 = 0.59$ (d), respectively, in the background of vorticities.

Nomenclatures

Scalars

a, b, C: Coefficients
d: The jet diameter at the inlet
e_l, e_h: Low and high limiting value
K: Turbulent kinetic energy
n: Number density
p: Fluid pressure
r, r^C: Radius, radial center
Re: Reynolds number
S: Swirl number
t: Time
u_x, u_θ: Axial and azimuthal velocity of fluids
u_i, u_j: Velocity of fluids
U_i, U_j: Mean velocities of fluids
U_0: The inflow velocity
x_i, x_j: Spatial variables
$\beta_1, \beta_2, \beta_3$: Regression lines
δ_{ij}: Kronecker function
Δt: Time step
Δx: Mesh spacing
ε_{ij}, E_{ij}: Turbulent energy dissipation tensor
$\varepsilon_1, \varepsilon_2, \varepsilon_3$: Three eigenvalues of ε_{ij}
η: The Kolmogorov length scale
λ: Inflow momentum thickness
ν: Kinematic viscosity of fluids
ν_T: Turbulent viscosity of fluids
τ_{ij}: Reynolds stress tensor.

Operators

∇: Hamiltonian operator, $\nabla = \mathbf{e}_i(\partial/\partial x_i)$
Δ: Laplace operator
∂_t: Partial derivative
$\langle\,\rangle$: Assemble averaging process
$p()$: Probability density function
$\delta()$: Infinitesimal increment
Σ: Summation operator.

Subscripts

c: Center
h: High
i, j: Index

l: Low
0: Initial
T: Turbulence
x: Axial direction
θ: Azimuthal direction
$'$: Fluctuation value
$\sim$: Eigenvalue.

Abbreviations

DNS: Direct numerical simulation
K-H: Kelvin-Helmholtz
PDF: Probability density function
VB: Vortex breakdown.

Conflict of Interests

The authors declare that there is no conflict of interests regarding the publication of this paper.

Acknowledgments

The authors are grateful for the support of this study by the National Natural Science Foundation of China (51106180), the Foundation for the Author of National Excellent Doctoral Dissertation of PR China (FANEDD, Grant no. 201438), and the China Postdoctoral Science Foundation (2013M540964).

References

[1] C. Chen and D.-J. Sun, "Numerical investigation of a swirling flow under the optimal perturbation," *Journal of Hydrodynamics Series B*, vol. 22, no. 5, supplement 1, pp. 237–241, 2010.

[2] Z. Wang and S. Q. Chen, "Structures of confined vortex breakdown in constant diameter pipe flow," *Journal of Hydrodynamics*, vol. 21, no. 3, pp. 341–346, 2009.

[3] S.-Y. Jin, Y.-Z. Liu, W.-Z. Wang, Z.-M. Cao, and H. S. Koyama, "Numerical evaluation of two-fluid mixing in a swirl micromixer," *Journal of Hydrodynamics*, vol. 18, no. 5, pp. 542–546, 2006.

[4] V. Shtern, M. Goldshtik, and F. Hussain, "Generation of swirl due to symmetry breaking," *Physical Review E: Statistical, Nonlinear, and Soft Matter Physics*, vol. 49, no. 4, pp. 2881–2886, 1994.

[5] B. di Pierro and M. Abid, "Instabilities of variable-density swirling flows," *Physical Review E—Statistical, Nonlinear, and Soft Matter Physics*, vol. 82, no. 4, Article ID 046312, 2010.

[6] M. R. Ruith, P. Chen, E. Meiburg, and T. Maxworthy, "Three-dimensional vortex breakdown in swirling jets and wakes: direct numerical simulation," *Journal of Fluid Mechanics*, vol. 486, pp. 331–378, 2003.

[7] L. Li, X. Y. Qiu, S. Jin, J. Xiao, and S.-Y. Gong, "Weakly swirling turbulent flow in turbid water hydraulic separation device," *Journal of Hydrodynamics B*, vol. 20, no. 3, pp. 347–355, 2008.

[8] N. Gui, J. Fan, K. Cen, and S. Chen, "A direct numerical simulation study of coherent oscillation effects of swirling flows," *Fuel*, vol. 89, no. 12, pp. 3926–3933, 2010.

[9] N. Gui, J. Fan, and S. Chen, "Numerical study of particle-vortex interaction and turbulence modulation in swirling jets," *Physical Review E—Statistical, Nonlinear, and Soft Matter Physics*, vol. 82, no. 5, Article ID 056323, 2010.

[10] N. Gui, J. Fan, and S. Chen, "The effects of flow structure and particle mass loading on particle dispersion in particle-laden swirling jets," *Physics Letters, Section A: General, Atomic and Solid State Physics*, vol. 375, no. 4, pp. 839–844, 2011.

[11] B. E. Launder and D. B. Spalding, "The numerical computation of turbulent flows," *Computer Methods in Applied Mechanics and Engineering*, vol. 3, no. 2, pp. 269–289, 1974.

[12] L. N. Jones, P. H. Gaskell, H. M. Thompson, X. J. Gu, and D. R. Emerson, "Anisotropic, isothermal, turbulent swirling flow in a complex combustor geometry," *International Journal for Numerical Methods in Fluids*, vol. 47, no. 10-11, pp. 1053–1059, 2005.

[13] D. R. Radenković, J. M. Burazer, and Đ. M. Novković, "Anisotropy analysis of turbulent swirl flow," *FME Transactions*, vol. 42, no. 1, pp. 19–25, 2014.

[14] A. Escue and J. Cui, "Comparison of turbulence models in simulating swirling pipe flows," *Applied Mathematical Modelling: Simulation and Computation for Engineering and Environmental Systems*, vol. 34, no. 10, pp. 2840–2849, 2010.

[15] D. X. Fu and Y. W. Ma, "A high order accurate difference scheme for complex flow fields," *Journal of Computational Physics*, vol. 134, no. 1, pp. 1–15, 1997.

[16] S. K. Lele, "Compact finite difference schemes with spectral-like resolution," *Journal of Computational Physics*, vol. 103, no. 1, pp. 16–42, 1992.

[17] A. Jameson and W. Schmidt, "Some recent developments in numerical methods for transonic flows," *Computer Methods in Applied Mechanics and Engineering*, vol. 51, no. 1–3, pp. 467–493, 1985.

[18] U. A. Krishnaiah, R. Manohar, and J. W. Stephenson, "Fourth-order finite difference methods for three-dimensional general linear elliptic problems with variable coefficients," *Numerical Methods for Partial Differential Equations*, vol. 3, no. 3, pp. 229–240, 1987.

[19] N. Gui, J. Yan, Z. Li, and J. Fan, "Direct numerical simulation of confined swirling jets," *International Journal of Computational Fluid Dynamics*, vol. 28, no. 1-2, pp. 76–88, 2014.

[20] N. Gui, J. R. Fan, and S. Chen, "Numerical study of particle-particle collision in swirling jets: a DEM-DNS coupling simulation," *Chemical Engineering Science*, vol. 65, no. 10, pp. 3268–3278, 2010.

[21] P. Moin and K. Mahesh, "Direct numerical simulation: a tool in turbulence research," *Annual Review of Fluid Mechanics*, vol. 30, pp. 539–578, 1998.

[22] I. Orlanski, "A simple boundary condition for unbounded hyperbolic flows," *Journal of Computational Physics*, vol. 21, no. 3, pp. 251–269, 1976.

[23] R. W. Johnson, *The Handbook of Fluid Dynamics*, CRC Press, New York, NY, USA, 1998.